4-7-2022

Modeling the Effects of Surface Roughness on Electron Yield

Trace Taylor
Utah State University

Matthew Robertson
Utah State University

JR Dennison
Utah State University

Modeling the Effects of Surface Roughness on Electron Yield

Trace Taylor, Matthew Robertson, and JR Dennison.

Materials Physics Group, Utah State University, Logan, Utah, 84322-4415, USA

***Abstract*— Surface conditions—including surface morphology, composition, contamination, and oxidation—can significantly affect electron yields and consequently spacecraft charging. The effects of surface roughness on electron yield are modeled in this study by considering four aspects of electron yield calculations: (i) simple models of rough surface geometry, (ii) the angular distributions of electrons emitted from various points on these surfaces, (iii) the likelihood of these emitted electrons escaping the rough surface, and (iv) the relative fractions of smooth and rough surfaces. Three simple periodic one-dimensional surface profiles were considered—namely rectangular, triangular, and sawtooth features; each surface profile was characterized by an aspect ratio of the surface feature width to the height. Two different angular emission profiles were considered for lower energy secondary electrons (a Lambertian cosine distribution) and higher energy backscattered electrons (a much narrower, energy-dependent screened Rutherford model approximating a Mott scattering cross-section which also depends on the atomic number of the material). In this initial study, only normally-incident electron profiles were considered, and any emitted electrons were assumed to be recaptured if they intersect any surface. The relative fractions of smooth and rough surfaces (which could in general have different yields for materials in these regions) were taken into account using a simple 1D "patch" model. Combining the surface profiles with the emission distributions allowed the calculation of a roughness coefficient—which predicted the effect of the surface profile on a smooth surface electron yield—for both secondary and backscattered yields for each surface geometry. Generalized predictions are presented for the reduced secondary and backscattered yields (scaled as the ratio of yields for materials in the smooth and rough fractions) as functions of aspect ratio and the fraction of the surface profile occupied by surface features. Results for backscattered electrons of different incident energies are also presented.**

I. Introduction

Spacecraft charging has been shown to be affected by several factors including temperature, radiation, contamination, and the morphology of the surface [1-4]. The purpose of this study was to investigate how surface roughness affects electron yield (EY) [2,5-11], which is a dominant contributor to spacecraft charging [8,11,12]. An EY may be generated from incident electrons, ions, or photons; however, electron-induced EYs are usually the most significant for spacecraft applications [11,14,15], so they were the focus of the study. Despite the recognized importance of surface roughness, simple models are not readily available to incorporate its effect on EY. This project develops a framework to evaluate roughness coefficients for basic surface geometry profiles suitable for inclusion in a simple "patch" model to account for the effects of roughness on EY [6,17].

II. Theoretical Model

When an incident electron collides with a material, it may interact with other electrons contained within the material. The incident electron may scatter back out of the material through a series of quasielastic collisions; these are known as backscattered electrons (BSE). Alternately, these collisions may impart enough energy to the materials to liberate electrons from within the material; these are known as secondary electrons (SE) [2,8,17].

In this initial study, only normally-incident electron profiles were considered. Emitted electrons were assumed to be recaptured if they subsequently intersected any surface. Thus, emitted electrons have a critical angle from the surface normal, θ_c, that determines whether they will be able to escape from the material [see Fig. 1(a)]. Surface roughness will act to decrease this critical angle from the maximum possible angle of 90° for a flat, smooth surface; as the critical angle decreases fewer electrons avoid collisions and thus more are re-absorbed, and the EY is consequently expected to decline [2,6,17]. The critical angles differ for scattering to the right or left as θ_R and θ_L, and are functions of the location of the incident electron collision along the lateral coordinate, X. All the information unique to the geometry of the periodic one-dimensional (1D) surface profiles considered here (namely rectangular, triangular, and sawtooth profiles) are thus contained in the expressions for $\theta_R(X)$ and $\theta_L(X)$, as functions of X.

The roughness model also requires expressions for the unnormalized angular distributions of emitted SE or BSE electrons, $A_n(\theta)$, from a point source at a position X. Two different angular emission profiles were considered for lower energy SE [a Lambertian cosine distribution; see Fig. 1(b)] and higher energy BSE [a screened Rutherford model, approximating a more accurate Mott scattering cross-section; see Fig. 1(c)] [17]. Operationally, SEs are defined as those with energies <50 eV, and BSEs are defined as those at higher energies >50 eV up to the incident energy, E_o [17]. The higher energy causes the BSE to potentially penetrate deeper within the material, causing roughness to have a lesser effect [8,11,17]. The BSE angular distribution is in general much narrower than the SE distribution. The screened Rutherford approximation incorporates a screening cutoff angle, which scales as $E_o^{1/2}$ and $\bar{\bar{Z}}^{1/3}$ [17]; this introduces a complex dependence for the roughness models for BSE on E_o and the mean atomic number, $\bar{\bar{Z}}$, as illustrated by the three angular distributions shown in Fig. 1(c) for 1.5 keV, 33 keV, and 100 keV incident electrons.

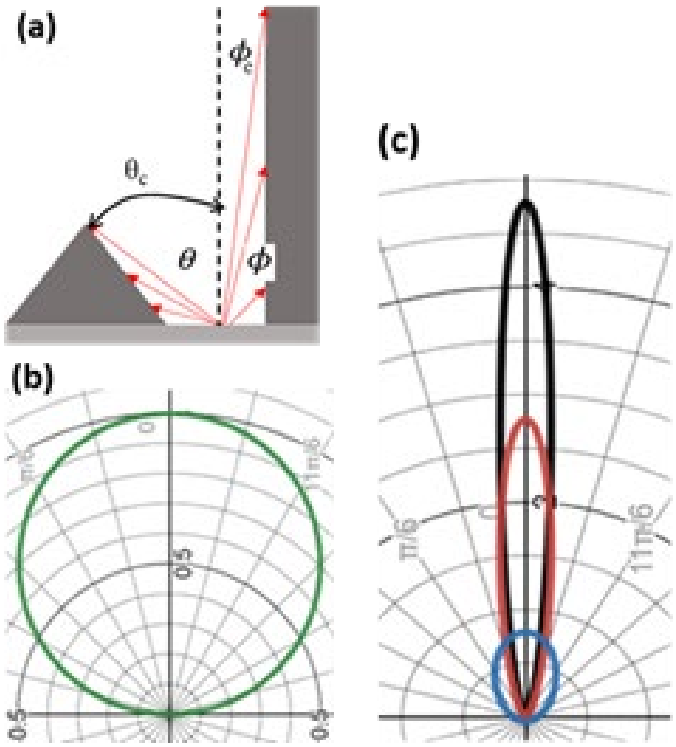

Fig.1. (a) Schematic of electron emission angles θ (low aspect ratio feature) and ϕ (high aspect ratio feature) originating from a point x laterally along a surface roughness feature. The critical angles are θ_c and ϕ_c Electron emission angular distribution functions. (b) Lambertian (cosine) distribution for SE yields. (c) Much narrower, energy-dependent screened Rutherford model approximating a Mott scattering cross-section which also depends on the atomic number of the material for BSE yields. Angular distributions shown are for 1.5 keV (**blue**), 33 keV (**red**), and 100 keV (**black**) incident electrons.

Finally, combining each surface profile with the SE or BSE emission distribution allowed the calculation of the fraction of electrons that can escape from a roughened surface as compared to a smooth, flat surface; this ratio is referred to as the roughness coefficient, $c_r(\alpha,\omega)$. This can be determined by integrating the appropriate normalized SE or BSE angular distribution function [the term in square brackets in (1)] for all allowed emitting an1gles $\theta_R(x) \le \theta \le \theta_L(x)$ over all lateral points $0 \le x \le \omega$ in the rough surface.

$$c_r(\omega,\alpha) = \omega \int_0^{\omega} \left\{ \int_{-\theta_L(x)}^{\theta_R(x)} \left[\frac{A_n(\theta)}{\int_{-\pi/2}^{\pi/2} A_n(\theta) d\theta} \right] d\theta \right\} dx \qquad (1)$$

where: (i) the reduced width, $\omega \equiv W/L$, is defined simply as the ratio of the lateral width of the roughness feature, W, to the total unit cell width, L; (ii) the aspect ratio, $\alpha \equiv W/D$, is defined as the ratio of W to the depth of the roughness feature, D; and (iii) the reduced lateral location of the incident electron collision, $x \equiv X/L$, is defined as the ratio of the X position to L.

The roughness coefficient, $c_r(\alpha,\omega)$, can be incorporated in a simple 1D "patch" model [16] of two-component composite material, where the relative fraction of the two constituent components—the smooth and rough surfaces—is $\omega \equiv W/L$. In general, the smooth and rough surfaces have different EY for materials in these regions; σ_s, δ_s, and η_s or σ_r, δ_r, and η_r, respectively. The reduced composite EY is

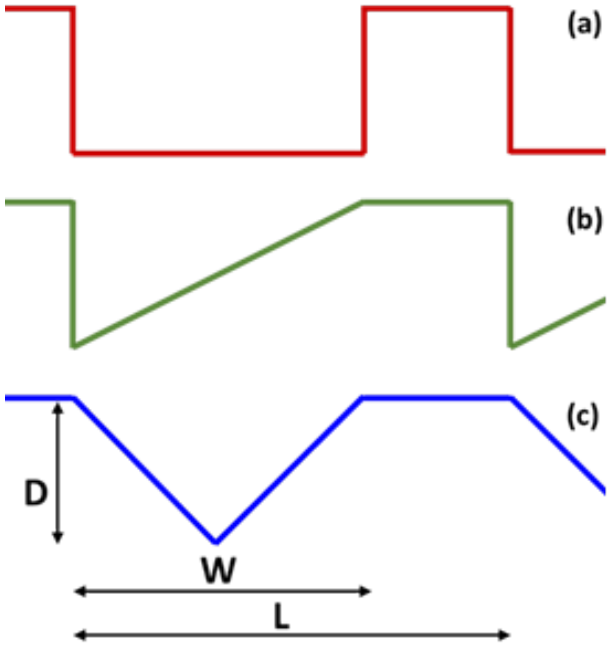

Fig. 2. Three periodic one-dimensional surface profiles considered here: (a) rectangular geometry, (b) sawtooth geometry. (c) triangular geometry. The surface feature width, W, and depth, D are indicated, as is the periodic unit cell length, L.

$$\tilde{\sigma}_{com}(\alpha,\omega) = (1-\omega) + \tilde{\sigma}_r \omega \, c_r(\alpha,\omega), \qquad (2)$$

written in terms of reduced composite and rough electron yields scaled to the smooth surface EY,

$$\tilde{\sigma}_{com} \equiv \sigma_{tot}/\sigma_s \quad \text{and} \quad \tilde{\sigma}_r \equiv \sigma_r/\sigma_s, \qquad (3)$$

with similar expressions for SE and BSE yields, δ_{com}, and η_{com}. The first term in (2), accounting for the contribution from the smooth surface, scales linearly with the relative fraction of smooth and rough surfaces, ω. The second term in (2), accounting for the contribution from the rough surface, is proportional to ω times the roughness coefficient, $c_r(\alpha,\omega)$, [which itself may be dependent on the aspect ratio, α, and/or ω through (1) and dependent on E_o and $\bar{Z}$ for BSE].

III. Results

Three simple, periodic 1D surface profiles were considered—namely rectangular, triangular, and sawtooth features—as shown in Fig. 2. Each surface profile was characterized by an aspect ratio of the surface feature width to the height and the relative fraction of smooth and rough surfaces, as shown in Fig. 3. The surface geometries were generalized by defining several reduced geometry coordinates, $x \equiv X/L$, $\alpha \equiv W/D$, and $\omega \equiv W/L$, based on the absolute coordinates.

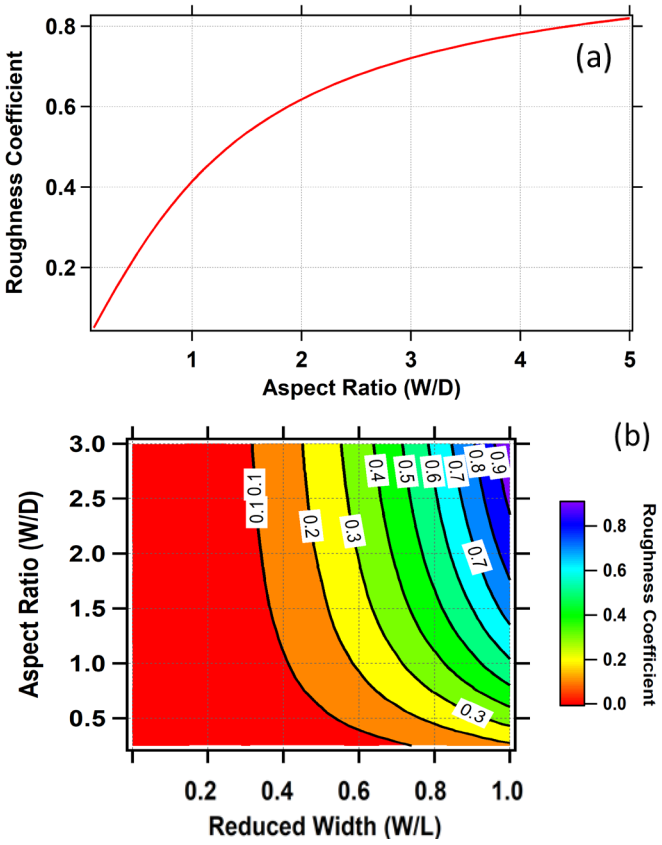

Fig. 3. Roughness coefficient as a function of aspect ratio and roughness fraction for the square well geometry model of surface roughness for (a) secondary electrons and (b) backscattered electrons.

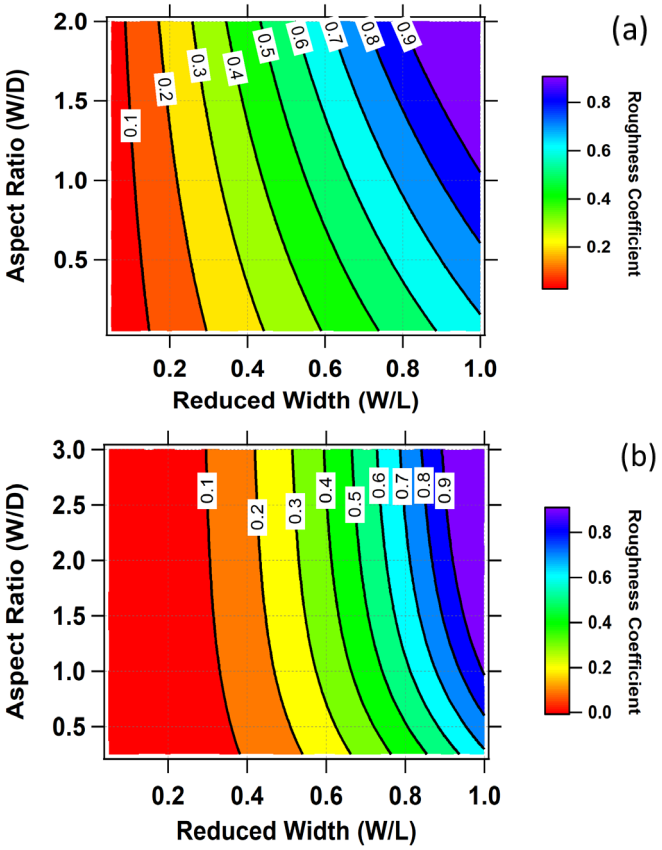

Fig. 4. Roughness coefficient as a function of aspect ratio and roughness fraction for the triangular geometry model of surface roughness for (a) secondary electrons and (b) backscattered electrons.

For each of these defined geometries, it is possible to develop analytic expressions for the left and right critical angles in terms of where the electron strikes, x, which are in turn inserted into (1) and integrated over the full geometry to determine roughness coefficient, $c_r(\alpha,\omega)$, for each geometry.

As expected, the rectangular model is the easiest to evaluate due to the even symmetry of the well and constant depth. It provided the simplest results, with $c_r(\alpha)$ dependent only on α:

$$c_{SE}(\alpha;R) = \left(\sqrt{1+\alpha^{-2}} - \alpha^{-1}\right), \tag{4}$$

as shown in Fig 3(a).

The equations for the critical angles for the triangular geometry are more complex, but the roughness coefficient can still be evaluated analytically given its even symmetry with a changing depth. It is given by

$$c_{SE}(\alpha,\omega;T) = \frac{\omega}{2\sqrt{2}}\left\{\left[1+\coth^{-1}\left(\sqrt{2}\right)\right] + \frac{\alpha}{\sqrt{2}}\left[1+\left(\omega/2\right)^2\right]^{-1/2}\right\} \tag{5}$$

as shown in Fig. 4(a).

Finally, the sawtooth geometry is the most complicated, as it lacks symmetry and has changing depth. The roughness coefficient is

$$c_{SE}(\alpha,\omega;S) = \frac{\alpha}{2}\left\{\left[\frac{\omega}{\sqrt{1+\alpha^2}}\right] + \int_0^{\omega}\left[\frac{x}{(\omega-x)\sqrt{1+\left(\frac{\alpha x}{\omega-\alpha}\right)^2}}\right]dx\right\} \tag{6}$$

Equation (5) was not able to be fully evaluated analytically, but numerical results for the triangular geometry SEY were obtained, as shown in Fig 5(a). The results for the SEY roughness coefficients for the three geometries as a function of aspect ratio, α, at $\omega \equiv W/L = 0.5$ are compared in Fig. 6(a).

Evaluation of (1) for the more complex BSE angular distributions were also evaluated numerically. BSEY results as a function of α and ω for the rectangular, triangular and sawtooth models are shown in Figs. 3(b), 4(b), and 5(b), respectively. Recall that the roughness coefficient for BSE has both energy and atomic number dependences through the screening cut-off angle. Figure 6(b) compares the roughness coefficients as a function of aspect ratio for the three geometries; these plots are evaluated at ω=0.5 for C (Z=6) at 1 keV, near the typical value for the peak BSE EY for most materials. Figure 6(c) compares the roughness coefficients as a function of incident energy for the three geometries; these

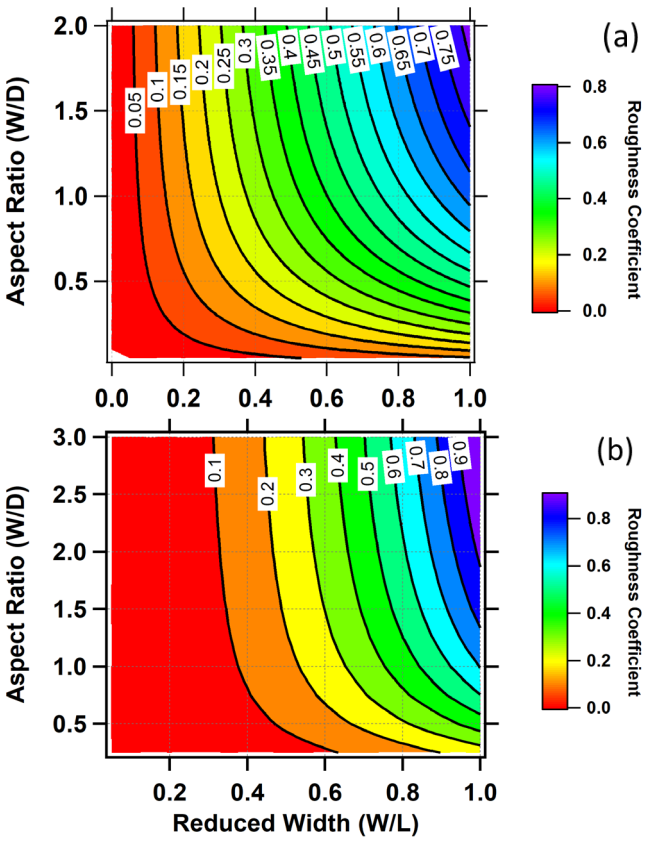

Fig. 5. Roughness coefficient as a function of aspect ratio and roughness fraction for the sawtooth geometry model of surface roughness (a) secondary electrons and (b) backscattered electrons.

plots are evaluated at α=3 and ω=0.5 for C (Z=6). A dashed green line in Fig, 6(c) indicates the approximate energy below which the BSE model becomes inaccurate for scattering below the screening cutoff angle. This is roughly 150 eV to 600 eV for elemental solids for 4≤Z≤92, and for most common spacecraft materials is only several times more than the operational lower bound of 50 eV for BSE and below the energy of the peak BSEY.

Figures 3, 4, and 5 summarize the EY results for (a) SE and (b) BSE for the rectangular, triangular, and sawtooth geometries, respectively. The plots show the roughness coefficient, $c_r(\alpha,\omega)$, from (2) as a function of aspect ratio, α, and roughness fraction, ω.

IV. Conclusions

Quantitative models to predict the effects of surface roughness on SEY and BSEY have been developed for three very general simple 1D models of rough surface geometry, each characterized by an aspect ratio of the surface feature width to the height and by the relative fractions of smooth and rough surfaces. The models predict a potentially large impact of surface roughness on EY under certain circumstances.

As expected, the aspect ratio was a dominant factor in the degree of EY suppression. There were clear differences predicted between the three geometries studied in the suppression of both SEY and BSEY. The roughness coefficient for a triangular well had a smaller impact on both SEY and

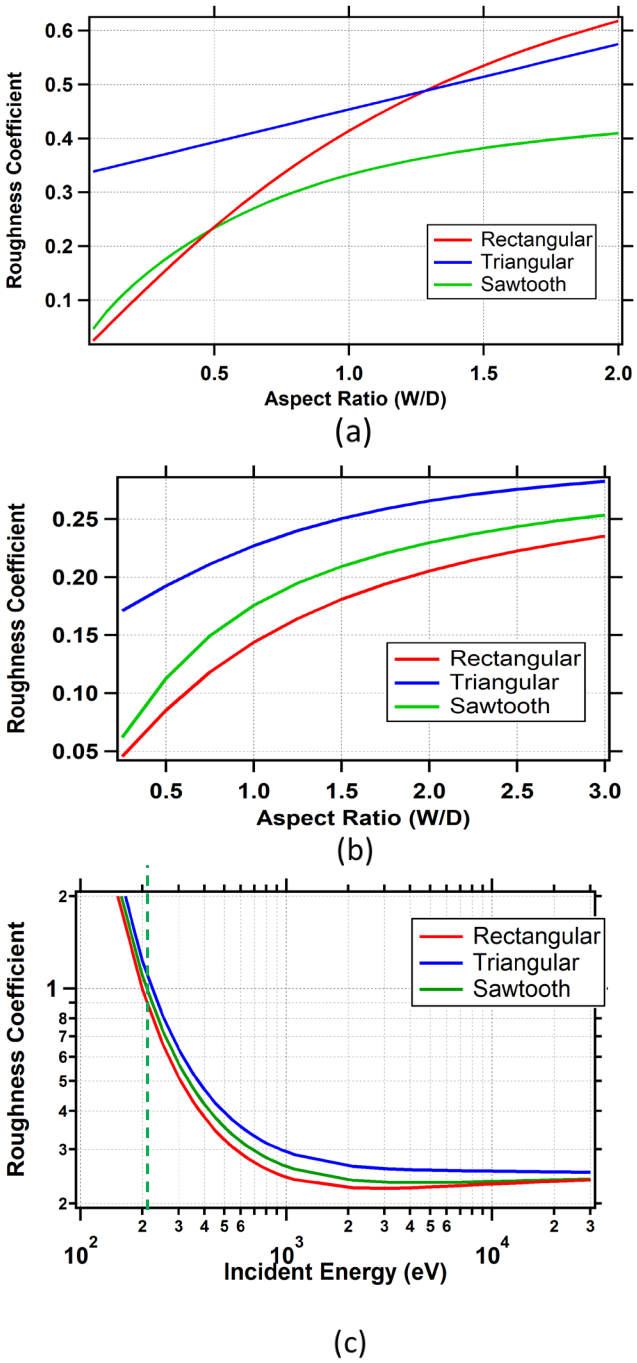

Fig. 6. Comparison of roughness coefficients for the three geometry models at a fixed ω=0.5. (a) Comparison of SEY roughness coefficients as a function of aspect ratio. (b) Comparison of the BSEY roughness coefficients as a function of aspect ratio, evaluated for C (Z=6) at 1 keV. (c) Comparison of BSEY roughness coefficients as a function of incident electron energy, evaluated at α=3 for C (Z=6). The dashed green line shows the approximate point below which the BSE model becomes inaccurate for scattering below the screening cutoff angle.

BSEY suppression. The rectangular well reduced BSEs the most and the sawtooth geometry reduced SEs the most. BSEY was significantly less affected by surface geometry than SEY, which is attributed to the deeper pentation of BSEs. Results for BSEY of different incident energies were also identified.

The proposed modeling of the effects of surface roughness on EY can be enhanced and extended in several ways. Work is

in progress to add additional 1D geometry models for hemispherical and sinusoidal roughness features. We also intend to extend the composite material EY models to incorporate 2D periodic surface structures [5] through 2D EY "patch" models [16], multilayer material EY models [18], and more than two constituent materials [16]. The angular distribution functions can be improved, especially for BSE, by incorporating specular reflection components based on non-normal scatter from roughness feature surfaces or from non-normal or isotropic electron incidence.

Additional work is in progress to test the efficacy of the proposed models for measured SEY and BSEY data for intentionally roughened Al and Cu surfaces [5], insulating Al_2O_3 particulate samples [19], and a very high aspect ratio carbon nanotube forest samples [20]. Initial results suggest the models are effective in determining the EY of various complex materials to within a reasonable margin of uncertainty. Indeed, it is clear that a key element of such applications will be in finding appropriate and accurate methods to characterize the sample surface roughness and which surface geometries are most applicable.

Acknowledgment

This work was partially supported through funding from a Utah State University Physics Department Blood/Taylor Undergraduate Research Fellowship and a USU Undergraduate Research and Creative Opportunities Grant (TT) and through a NASA Utah Space Grant Consortium Graduate Fellowship (MR).

References

[1] Hastings, D., and H. Garrett, *Spacecraft-Environment Interactions*, (Cambridge University Press, Cambridge, UK), 2004.

[2] Bronstein, I. M., J. Moiseevich, and B. S. Freiman, "Secondary electron emission" Moscow, Russia: Atomizdat, 408 (rus), 1969.

[3] Dennison, JR, "The Dynamic Interplay Between Spacecraft Charging, Space Environment Interactions and Evolving Materials," *IEEE Tran. Plasma Science*, vol. 43, no. 9, pp. 2933-2940, 2015.

[4] Chang, W.Y., J.R. Dennison, J. Kite and R.E. Davies "Effects of Evolving Surface Contamination on Spacecraft Charging," *Proc. 38th American Institute of Aeronautics and Astronautics Meeting on Aerospace Sciences*, Reno, NV, Paper AIAA-2000-0868, Jan., 2000.

[5] Taylor, T., M. Robertson, and JR Dennison, "Effects of Surface Roughening on Electron Yields of Polished Cu and Al Samples," *USU Student Research Symposium*, Logan, UT, April, 2021.

[6] Taylor, T., M. Robertson, and JR Dennison, "Models of Electron Yield Roughness Coefficient," *Am. Physical Society Four Corners Meeting,* University of Colorado-Boulder, Boulder, CO, Virtual Meeting, Oct., 2021.

[7] Olano, L, M. E. Dávila, JR Dennison, P. Martín-Iglesias, and I. Montero, "Dynamic secondary electron emission in rough composite materials," *Science Reports,* vol. 9, Article number: 13967, 2019.

[8] Lundgreen, P., J.R. Dennison, "Strategies for determining electron yield material parameters for spacecraft charge modeling". *Space Weather*, vol. 18, 2020.

[9] Baglin, V., J. Bojko, C. Scheuerlein, O. Gröbner, M. Taborelli, B. Henrist, and N. Hilleret, "The secondary electron yield of technical materials and its variation with surface treatments," *Proc. EPAC 2000*, Vienna, Austria, 2000.

[10] Hu, X.-C., Meng Cao, Wan-Zhao Cui, "Influence of surface topography on the secondary electron yield of clean copper samples," *Micron*, vol. 90, pp. 71-77, 2016.

[11] Inguimbert, C, J. Pierron, M. Raine, M. Belhaj, and J. Puech, "GEANT4 Study of the effect of the surface roughness on the Secondary Emission Yield." Sources, Interaction with Matter, Detection and Analysis of Low Energy Electrons 2017, Pula, Sardinia, September 2017.

[12] Dennison, JR, R.C. Hoffmann, and J. Abbott, "Triggering Threshold Spacecraft Charging with Changes in Electron Emission from Materials," *Proc. 45th Am. Instit. of Aeronautics and Astronautics Meeting on Aerospace Sciences*, Paper AIAA-2007-1098, 16 pp., Reno, NV, January, 2007.

[13] Dennison, JR, "Modifications of Electron Yield Due to Interactions with the Space Environment," *Proc. 16th Spacecraft Charging Tech. Conf.,* Cocoa Beach FL, USA, April, 2021.

[14] Gussenhoven, M. and E. Mullen, A 'worst case' spacecraft charging environment as observed by SCATHA, *20th Aerospace Sciences Meeting*, April, 1979.

[15] Olsen, R. C., "A threshold effect for spacecraft charging." *J. Geophysical Res.: Space Physics*, vol. 88(A1), pp. 493-499, 1983.

[16] Robertson, M., T. Taylor, T. Keaton, and JR Dennison, "Analysis of Extrinsic Factors on Electron Yield with a "Patch" Model," *Appl. Space Environ. Conf. 2021*, Jet Propulsion Laboratory, Pasadena, CA, Virtual Meeting, Nov., 2021.

[17] Reimer, L., Scanning Electron Microscopy. *Physics of Image Formation and Microanalysis*, (Springer-Verlag, New York), 1985.

[18] Wilson, G., M. Robertson, J. Lee, and JR Dennison, "Electron Yield Measurements of Multilayer Conductive Materials," *Proc. Applied Space Environments Conf. 2019,* (Los Angeles, CA, May, 2019).

[19] Keaton, T. and JR Dennison, "Environmental Charging of the Lunar Regolith: Electron Yield Measurements of Alumina Particulates," *NASA Workshop on Fundamental and Applied Lunar Surface Research in Physical—Sciences Session 10: Fundamental and Applied Lunar Surface Research in Physical Sciences (Virtual),* NASA Lunar and Planetary Institute, Houston, TX, August, 2021.

[20] Wood, B., J. Lee, G. Wilson, T.-C. Shen and J. R. Dennison, "Secondary Electron Yield Measurements of Carbon Nanotube Forests: Dependence on Morphology and Substrate," *IEEE Trans. on Plasma Sci*., vol. 47, no. 8, pp. 3801-3809, 2019.